Isovector giant quadrupole resonance observed in $^{30}Si(\vec{p},\gamma)^{31}P$

G. Feldman, L. H. Kramer, and H. R. Weller
Duke University, Durham, North Carolina 27706
and Triangle Universities Nuclear Laboratory, Durham, North Carolina 27706

E. Hayward* and W. R. Dodge†
National Institute of Standards and Technology, Gaithersburg, Maryland 20899
(Received 15 February 1990)

The $^{30}Si(\vec{p},\gamma)^{31}P$ reaction has been studied in the proton energy range $E_p=20-36$ MeV. Angular distributions of the cross section and the analyzing power have been measured for γ-ray transitions to the ground state and the first excited state of ^{31}P over the angular range 37.5°–145° at $E_p=25.5$ MeV. Legendre polynomial fits to both observables yield nonzero coefficients of order $k=3,4$, suggesting the interference of $E2$ radiation with the dominant $E1$ radiation. A transition-matrix-element analysis of the data indicates that ~26% of the γ_1 cross section at this energy arises from $E2$ radiation, whereas only 10% of the γ_0 cross section can be attributed to $E2$ radiation. Direct-semidirect calculations give a direct $E2$ component of ~7% for both channels, suggesting significant excess $E2$ strength in the γ_1 channel at this energy. The energy dependence of the 90° analyzing power for γ_1 shows a resonance structure near $E_p=34$ MeV which can be reproduced by a direct-semidirect calculation including an $E2$ resonance at $E_{GQR}=38.6$ MeV with a width of $\Gamma_{GQR}=5.0$ MeV and a strength of 50% of the isovector $E2$ energy-weighted sum rule. The current results thus provide strong evidence for collective $E2$ strength roughly at the expected peak of the isovector giant quadrupole resonance built on the first excited state of ^{31}P.

I. INTRODUCTION

Polarized proton capture has the potential to be a valuable tool in mapping out resonant multipole strength distributions at high excitation. In the present paper, we have used this technique to study $E2$ strength in ^{31}P. The current work is an extension of the experiment of Cameron *et al.*[1,2] to higher energy. The previous work studied the $^{30}Si(p,\gamma)^{31}P$ reaction with unpolarized protons up to $E_p=28$ MeV and with polarized protons up to $E_p=15$ MeV. This earlier work[2] suggested the presence of significant $E2$ strength above the giant dipole resonance (GDR), based on the observed energy dependence of the fore-aft asymmetry of the cross section. To pursue this issue, we have measured the cross section $\sigma(\theta)$ and the vector analyzing power $A_y(\theta)$ at nine points in the angular range $\theta_\gamma=37.5°-145°$ for the $^{30}Si(\vec{p},\gamma)^{31}P$ reaction using polarized protons at $E_p=25.5$ MeV. A model-independent analysis using transition matrix elements was employed to obtain quantitative results for the $E2$ fraction present in capture to the ground state (γ_0) and the first excited state (γ_1) of ^{31}P at this energy. We have also measured the vector analyzing power at $\theta_\gamma=90°$ at 11 energies over the proton energy range $E_p=20-36$ MeV. Theoretical work[3] based on the direct-semidirect model has suggested that the 90° analyzing power is especially sensitive to the presence of the isovector giant quadrupole resonance (IVGQR).

Similar work on the $^{15}N(\vec{p},\gamma_0)^{16}O$ reaction by Kovash *et al.* has revealed that whereas (5±1)% of the capture cross section at 35 MeV excitation in ^{16}O can be attributed to $E2$ radiation, this fraction rises to (11±1)% at 39 MeV excitation.[4] To determine the significance of this $E2$ strength requires an absolute $E2$ cross section, since the $E2$ fraction is affected by the energy dependence of the much larger $E1$ cross section, which is falling rapidly with the tail of the giant dipole resonance. Based on measurements of the absolute (p,γ) cross section for this reaction,[5] which give $A_0=0.558\pm0.022$ μb/sr and 0.319 ± 0.013 μb/sr for $E_x=35$ and 39 MeV, respectively, the data points from Ref. 4 correspond to absolute $E2$ cross sections of 0.028 ± 0.005 μb/sr and 0.035 ± 0.003 μb/sr, suggesting an increase in the $E2$ cross section with increasing energy in this region. These results, which were based on a reaction amplitude analysis, constitute model-independent evidence for significant $E2$ strength in the expected vicinity of the IVGQR in ^{16}O.

The only previous measurements of the energy dependence of the vector analyzing power have been performed at lower energies ($E_p\leq18$ MeV) in the $^{14}C(\vec{p},\gamma_0)^{15}N$ reaction by Snover *et al.*[6] and in the $^{15}N(\vec{p},\gamma_0)^{16}O$ reaction by Hanna *et al.*[7] In the former work, no evidence of a resonance was found. In the latter work, $E2$ strength located slightly above the centroid of the GDR was tentatively identified as isovector in nature, but the energy range was insufficient to obtain a complete excitation function over the entire region of the IVGQR in ^{16}O. In the current work, we have spanned the expected energy region of the IVGQR in ^{31}P, and we present, for the first time, definitive results that identify a compact IVGQR in a light nucleus using the polarized proton capture reaction as a tool.

II. EXPERIMENTAL DETAILS

The present data for the $^{30}Si(\vec{p},\gamma)^{31}P$ reaction were taken at the 88-Inch Cyclotron of the Lawrence Berkeley Laboratory. Polarized proton beams were incident on a 10 mg/cm^2 self-supporting ^{30}Si target enriched to 95%. Capture γ rays were detected in a new 25.4 cm×27.9 cm NaI detector with active plastic-scintillator (NE110) anticoincidence shield. The detector was surrounded by 10 cm of Pb shielding, 20 cm of boric acid bricks to moderate neutrons from the target, and 2.5 cm of ^{6}LiH to absorb thermal neutrons. The front face of the detector was located ~1.2 m from the target, and a collimator in the front Pb shield defined the γ-ray acceptance angle. For additional neutron shielding, the collimator held a plastic plug, and a 25 cm wall of paraffin was placed between the target and the NaI detector. The setup of the spectrometer is similar to the system used at the Triangle Universities Nuclear Laboratory, for which the details have been described elsewhere.[8] Data were taken in pulsed-beam mode, utilizing the time structure of the cyclotron beam. Time gates were set in a time-of-flight spectrum so as to eliminate neutron-induced backgrounds from the γ-ray spectra.

In the angular distribution measurement, the beam polarization ($P\sim68\%$) was determined via the $^4He(\vec{p},p)^4He$ elastic-scattering reaction, for which the analyzing powers in this energy region are well known.[9] The polarization was monitored during the course of the experiment by measuring the up-down asymmetry of protons scattered by the ^{30}Si target using two solid-state detectors located symmetrically on either side of the beam axis. Despite the fact that the analyzing powers for elastic proton scattering from ^{30}Si are not known, this procedure provided a relative check of the beam polarization. We found the polarization to drop by 10% of its value (from 68% to 61%) over the running period of 5 days. For the energy-dependence measurement, the beam polarization ($P\sim58\%$) was obtained in the same manner. In this case, however, the polarization was checked at each energy using the $^4He(\vec{p},p)^4He$ reaction. The effect of variable polarization was included in all reported values of the analyzing power for the capture reaction.

III. ANALYSIS AND RESULTS

A. Angular distributions

An example of a raw pulse-height distribution measured at $\theta_\gamma=50°$ is given in the top panel of Fig. 1. Several strong γ-ray transitions are clearly resolved in this spectrum. The high-energy portion of such a distribution is shown in the lower panel of Fig. 1. The spectrum was fitted with NaI line shapes located at the positions of the first seven strong single-particle states in ^{31}P (up to $E_x=5.02$ MeV), as given by (^{3}He,d) proton stripping results.[10] The figure shows the individual fits to the γ_0 and γ_1 transitions explicitly (dashed curves), along with the total fit to the spectrum (solid curve). Transition strengths were obtained by integrating the response function down to zero energy—a linear extrapolation to zero was used below the point to which the NaI response is known. All yields were subsequently corrected for accidental rejection of good γ-ray events by the anticoincidence shield and for deadtime effects.

The angular distributions of the relative cross section $\sigma(\theta)/A_0$ and the product of analyzing power and relative cross section $\sigma(\theta)A_y(\theta)/A_0$ for γ_0 and γ_1 are plotted in Fig. 2. Both cross sections are strongly forward peaked, implying significant mixing of opposite parity radiation ($M1$ or $E2$) with the dominant electric dipole ($E1$) radiation. The analyzing power for γ_1 is large, especially at 90°, but for γ_0 it is small at all angles. The analyzing power for γ_1 also deviates substantially from the typical $\sin(2\theta)$ angular dependence expected for pure $E1$ radiation.

The angular distribution of the cross section has been expressed as an expansion in Legendre functions up to order $k=4$:

$$\sigma(\theta)/A_0=1+\sum_{k=1}^{4} a_k Q_k P_k(\theta) ,$$

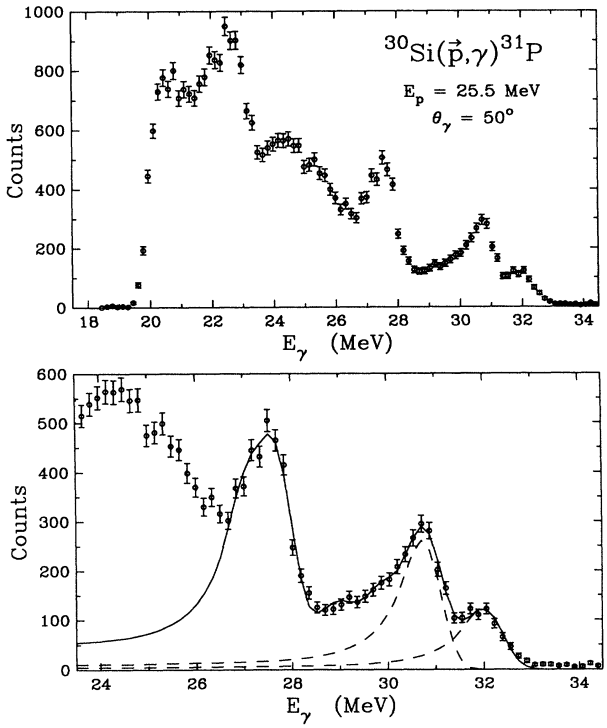

FIG. 1. Upper panel: Measured γ-ray spectrum for the $^{30}Si(\vec{p},\gamma)^{31}P$ reaction at $E_p=25.5$ MeV ($\theta_\gamma=50°$). Strong transitions are evident to the ground state and first excited state ($E_x=1.27$ MeV), as well as to groups of states near $E_x=4.4$, 7.0, and 9.5 MeV. The spectrum cutoff at $E_\gamma=20$ MeV is due to the electronic discriminator setting. Lower panel: High-energy portion of the above spectrum, showing the total lineshape fit (solid curve) to the data. The total fit accounts for γ-ray transitions to the first seven strong single-particle states in ^{31}P (up to $E_x=5.02$ MeV). The positions of the γ_0 and γ_1 transitions are shown explicitly (dashed curves).

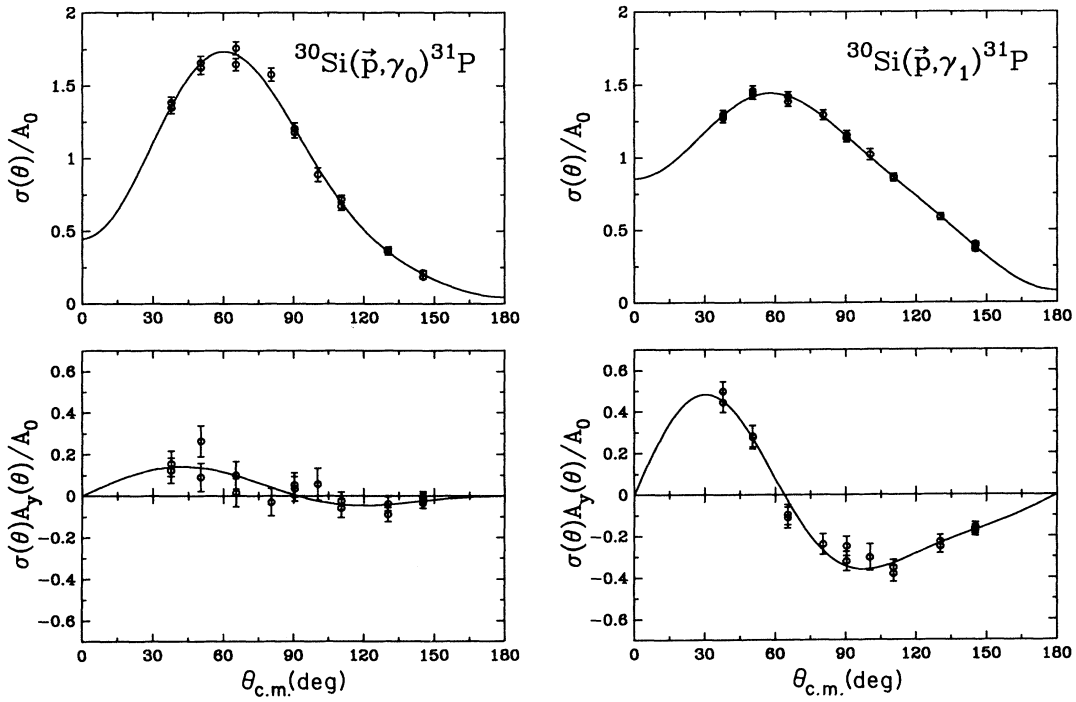

FIG. 2. Angular distributions of cross section and analyzing power for the γ_0 (left panel) and γ_1 (right panel) transitions from the ^{30}Si($\vec{p},\gamma$)^{31}P reaction at $E_p=25.5$ MeV. The solid curves are the Legendre polynomial fits to the data, the results of which are given in Table I.

and that of the product of vector analyzing power and cross section as an expansion in associated Legendre functions:

$$\sigma(\theta)A_y(\theta)/A_0=\sum_{k=1}^{4} b_k Q_k P_k^1(\theta) ,$$

where the Q_k are the usual finite geometry correction factors.[11] The least-squares fits to the data are shown by the solid curves in Fig. 2, and the resulting angular distribution coefficients a_k and b_k are presented in Table I. Finite values for the odd coefficients indicate the interference of multipoles of opposite parity, and nonzero values of the Legendre coefficients of order $k=3,4$ suggest that the interfering amplitudes originate primarily from $E2$ radiation (rather than $M1$).

TABLE I. Coefficients a_k and b_k obtained from the Legendre polynomial fits to the angular distributions of cross section and analyzing power for transitions to the ground state and first excited state of ^{31}P from the ^{30}Si($\vec{p},\gamma$)^{31}P reaction at $E_p=25.5$ MeV.

Coefficient	^{30}Si($\vec{p},\gamma_0$)^{31}P	^{30}Si($\vec{p},\gamma_1$)^{31}P
a_1	0.75±0.02	0.56±0.01
a_2	−0.58±0.03	−0.40±0.03
a_3	−0.55±0.04	−0.17±0.03
a_4	−0.18±0.04	−0.13±0.04
b_1	0.03±0.02	−0.16±0.01
b_2	0.06±0.01	0.18±0.01
b_3	0.02±0.01	0.12±0.01
b_4	0.00±0.01	0.04±0.01

To obtain a model-independent estimate of the contributing amplitudes, we have performed a transition-matrix-element (TME) analysis of these angular distributions, assuming only $E1$ and $E2$ terms. Whereas $M1$ radiation cannot, in principle, be completely excluded, it is not expected to contribute significantly in this energy region, as discussed in Ref. 1. An intermediate continuum state I is formed by coupling the projectile angular momentum $j=l+s$ to the target spin J_i; the final state J_f is reached by the emission of $E\lambda$ radiation. The complex reduced transition matrix elements (denoted by T) can then be written in terms of a real amplitude R and a phase ϕ:

$$T=\langle J_f\|E\lambda\|(ls)j\times J_i=I\rangle\equiv Re^{i\phi} .$$

For $E1$ capture to the $\frac{3}{2}^+$ first excited state of ^{31}P at $E_x=1.27$ MeV (primarily a $1d_{3/2}$ single-particle state, with spectroscopic factor[10] $C^2S=0.63$), there are three possible partial waves ($^2p_{1/2}$, $^4p_{3/2}$,$^6f_{5/2}$) that can contribute. The notation $^{2I+1}l_j$ refers to the orbital angular momentum l and the total angular momentum j of the projectile, and the spin I of the intermediate state. For $E2$ capture, there are four possible partial waves

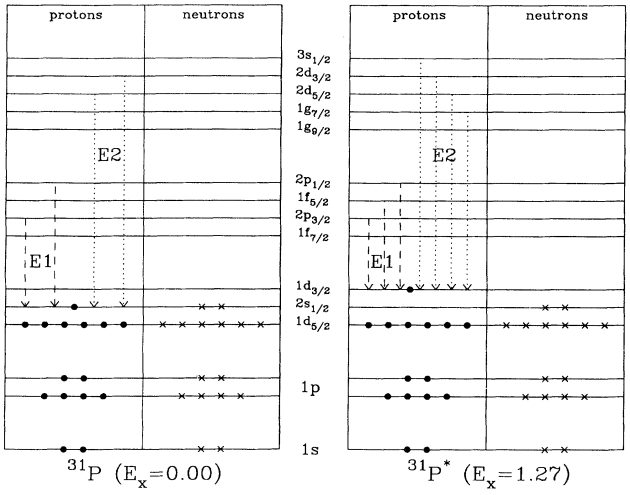

FIG. 3. Schematic representation of the allowed $E1$ and $E2$ single-particle transitions to the ground state (left panel) and first excited state (right panel) of ^{31}P from the ^{30}Si$(\vec{p},\gamma)^{31}$P reaction. The $E1$ transitions are indicated by dashed lines; the $E2$ transitions are given by dotted lines.

($^2s_{1/2}$, $^4d_{3/2}$, $^6d_{5/2}$, $^8g_{7/2}$). Transitions to the $\frac{1}{2}^+$ ground state (primarily a $2s_{1/2}$ single-particle state, with spectroscopic factor[10] $C^2S=0.48$) are considerably simpler ($^2p_{1/2}$ and $^4p_{3/2}$ for $E1$; $^4d_{3/2}$ and $^6d_{5/2}$ for $E2$). The allowed $E1$ and $E2$ transitions to the ground state and first excited state of ^{31}P are illustrated schematically in Fig. 3.

The relationships between the transition matrix elements and the angular distribution coefficients a_k and b_k in jj coupling have been previously deduced.[12] These are given explicitly in Ref. 1 for the ground-state transition and in the Appendix for the first-excited-state transition. Using these relationships, the amplitudes and phases of the TME's were treated as free parameters and were varied in a χ^2-minimization routine based on MINUIT (Ref. 13) to fit the cross section and analyzing power data *simultaneously*. The quality of the fits was identical to that obtained when fitting in terms of Legendre polynomials.

The results of the TME analysis are given in Table II. Each column corresponds to a possible solution; all of the solutions for each final state give equivalently good fits. The quantities listed in the table represent the percentage of the total cross section contributed by each partial wave. For the γ_0 case, two solutions are possible that give similar χ^2 values, but the $E2$ strength fraction (10%) is independent of the solution. Based on the absolute cross section of Cameron *et al.*,[1] this result corresponds to $\sigma_{E2}(p,\gamma_0)=0.05\pm0.01$ μb/sr.

The γ_1 case gives multiple solutions with similar χ^2 values which were found after an exhaustive search of the χ^2 space defined by the free parameters. These solutions fall into general classes which are represented in Table II, but we have chosen the leftmost two shown in the table as being the most physically plausible, based on simple shell-model considerations that favor $l\rightarrow l+1$ $E1$ transitions and $l\rightarrow l+2$ $E2$ transitions. In this case, the $E2$ cross section is $\sigma_{E2}(p,\gamma_1)=0.30$–$0.48$ μb/sr. Despite the uncertainty (20–32%) in the $E2$ percentage, it is clear that substantial $E2$ contributions arise in (p,γ_1) at this energy, more than twice as much as in (p,γ_0). Direct-semidirect model calculations indicate that direct $E2$ capture can account for only $\sim$7% of the cross section for both γ_0 and γ_1 at this energy, suggesting the presence of substantial excess $E2$ strength in the γ_1 channel.

B. Energy dependence

Another issue to address is the variation of the $E2$ absolute cross section with energy. The fact that the fractional $E2$ strength changes is not sufficient to infer anything about the importance of $E2$ radiation since variations in the $E1$ cross section will also affect the $E2$ fraction. This is clear by examining the TME analysis of the earlier Cameron data at $E_p=11$ and 15 MeV (see Table III). In the case of γ_0, the $E2$ fractions for $E_p=11$ and 15 MeV (2% and 4.6%, respectively) are lower than at $E_p=25.5$ MeV (10%), but the absolute $E2$ cross sections

TABLE II. Results of the transition-matrix-element analysis for capture to the ground state and first excited state of ^{31}P. Each column corresponds to a different solution. The quantities represent the percentage contribution of each partial wave to the total cross section. The total strength of each multipole ($E1$ or $E2$) is given at the bottom of the column.

Partial Wave	^{30}Si$(\vec{p},\gamma_0)^{31}$P		^{30}Si$(\vec{p},\gamma_1)^{31}$P					
$^2p_{1/2}(E1)$	2	72	34	7	21	45	8	21
$^4p_{3/2}(E1)$	88	18	7	10	17	2	5	26
$^6f_{5/2}(E1)$			39	51	24	34	46	20
$\sum(E1)$	90	90	80	68	62	81	59	67
$^2s_{1/2}(E2)$			1	8	32	12	14	4
$^4d_{3/2}(E2)$	1	8	3	10	3	3	17	8
$^6d_{5/2}(E2)$	9	2	3	0	0	1	3	19
$^8g_{7/2}(E2)$			13	14	3	3	7	2
$\sum(E2)$	10	10	20	32	38	19	41	33

TABLE III. Values of the absolute (p,γ) cross sections (from Ref. 1), the $E2$ strength fractions, and the resulting absolute $E2$ cross sections for capture to the ground state and first excited state of ^{31}P at proton energies $E_p = 11$, 15, and 25.5 MeV.

	^{30}Si$(\vec{p},\gamma_0)^{31}$P			^{30}Si$(\vec{p},\gamma_1)^{31}$P		
E_p (MeV)	A_0 (μb/sr)	$E2$ fraction (%)	σ_{E2} (μb/sr)	A_0 (μb/sr)	$E2$ fraction (%)	σ_{E2} (μb/sr)
11.0	7.3±0.1	2±1	0.15±0.08	6.9±0.1	1–13	0.07–0.90
15.0	3.6±0.1	4.6±0.5	0.17±0.02	8.5±0.1	1–20	0.09–1.70
25.5	0.53±0.04	10±1	0.05±0.01	1.5±0.1	20–32	0.30–0.48

are higher than at $E_p = 25.5$ MeV by about a factor of 3.

The case of γ_1 is considerably more complicated, due to the seven contributing partial waves for $E1$ and $E2$ capture. At $E_p = 11$ MeV, solutions of 8–13% $E2$ contributions give $\chi^2 \approx 10.5$; however, other solutions of ~2% $E2$ strength give $\chi^2 \approx 12.5$, and even pure $E1$ solutions ($\chi^2 \approx 14.5$) are marginally acceptable. Similar results are obtained for the analysis of γ_1 at $E_p = 15$ MeV. Thus, although a well-defined value of the $E2$ cross section cannot be specified, the overall picture (as seen in Table III) does not rule out an increase in the $E2$ cross section between $E_p = 11$–15 MeV and $E_p = 25.5$ MeV. Unfortunately, a more quantitative result is not presently available.

The energy dependence of $A_y(90°)$ for the ground-state and first-excited-state transitions is shown in Fig. 4. The absolute value of the 90° analyzing power for γ_1 is sizable and increases monotonically over most of the measured energy range, reaching a peak at $E_p = 34$ MeV. No such peaking behavior is evident in the γ_0 case, however, and the analyzing power is nearly zero at all energies.

We have used the direct-semidirect (DSD) model to calculate $A_y(90°)$ as a function of energy. In these calculations, we have included the giant dipole resonance as well as isoscalar and isovector components of the giant quadrupole resonance. For the isovector interaction, a complex particle-vibration coupling form factor was used, with a real volume term of strength $V_1 = 70$ MeV and an imaginary surface term of strength $W_1 = 35$ MeV. The isoscalar quadrupole coupling interaction was treated as a real surface-peaked form of strength $U_0 = -50$ MeV. Optical model parameters were obtained from the global fits of Becchetti and Greenlees.[14] The bound-state potential well depth was adjusted to obtain the correct binding energy. Based on the previous work of Cameron *et al.*,[1] a two-component GDR (due to isospin splitting) was used with the following parameters: $E_< = 17.3$ MeV, $\Gamma_< = 3.4$ MeV, $S_< = 54\%$ and $E_> = 20.6$ MeV, $\Gamma_> = 4.0$ MeV, $S_> = 46\%$. The isoscalar quadrupole resonance was included with $E = 19.7$ MeV, $\Gamma = 7.1$ MeV, and $S = 32\%$.[15] The resonance parameters of the IVGQR were treated as free parameters in order to fit the energy dependence of $A_y(90°)$ for the γ_1 transition. No such fitting procedure was employed for the γ_0 transition.

The solid curves in Fig. 4 are the results of the above DSD calculations, including the IVGQR with energy $E_{GQR} = 38.6 \pm 1.0$ MeV and width $\Gamma_{GQR} = 5.0 \pm 1.2$ MeV, and exhausting (50±15)% of the isovector $E2$ energy-weighted sum rule. The dashed curves are the same calculations but without the IVGQR. The γ_0 transition shows no particular distinction between the two calculations. While the energy dependence is nearly flat, the calculated magnitude of $A_y(90°)$ for γ_0 is small but nonzero, in marginal agreement with the data. The peaking behavior of $A_y(90°)$ for the γ_1 transition, however, is reproduced by the DSD calculation including the IVGQR, in

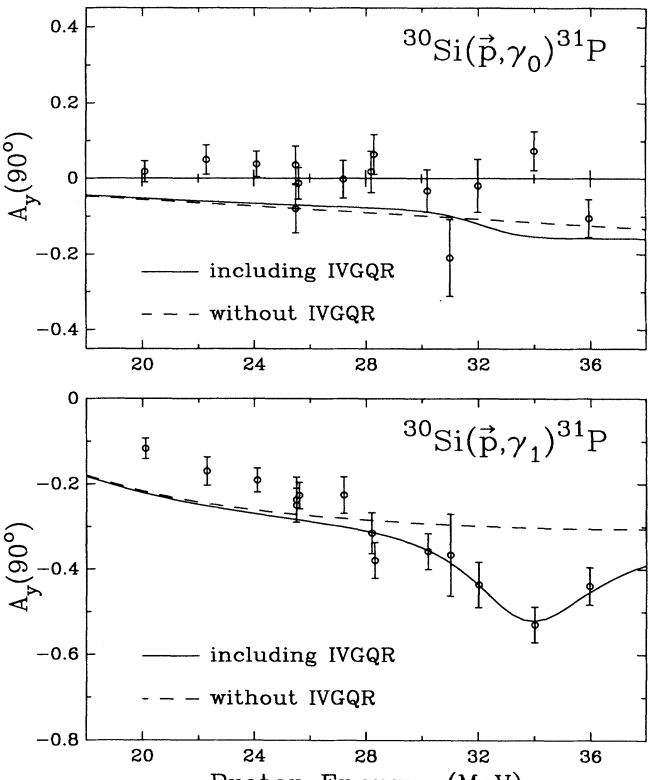

FIG. 4. Energy dependence of the 90° analyzing power for the γ_0 (top panel) and γ_1 (bottom panel) transitions from the ^{30}Si$(\vec{p},\gamma)^{31}$P reaction. The curves are direct-semidirect calculations that either include the IVGQR (solid curves) or neglect it (dashed curves). The parameters for the IVGQR were obtained by fitting the γ_1 excitation function and are discussed in the text.

contrast with the smooth energy variation of the curve with no $E2$ resonance. Clearly, in the γ_1 case, the need for a localized (collective) enhancement of $E2$ strength in this higher-energy region is apparent.

IV. CONCLUSION

In summary, we have studied the $^{30}\mathrm{Si}(\vec{p},\gamma)^{31}\mathrm{P}$ reaction over the proton energy range $E_p=20-36$ MeV using polarized protons, corresponding to excitation energies of $E_x=26.6-42.1$ MeV in ^{31}P. A transition-matrix-element analysis of the angular distributions of the cross section and the analyzing power at $E_p=25.5$ MeV has revealed the presence of considerable $E2$ strength at 32 MeV excitation energy in ^{31}P. We find that $E2$ radiation accounts for 10% of the total cross section for γ_0 and $\sim$26% for γ_1. For γ_1, in particular, the data suggest a sizable concentration of $E2$ strength at this energy, well in excess of the direct $E2$ capture strength ($\sim$7%) predicted by the direct-semidirect model. Thus, these results provide strong evidence for collective $E2$ strength in the γ_1 channel. Somewhat surprisingly, the γ_0 channel does not show a similar result. In that case, direct $E2$ capture alone can account for the observed $E2$ strength in the cross section.

The energy dependence of $A_y(90°)$ reveals a strong signal for the presence of substantial collective $E2$ strength located near $E_p=34$ MeV ($E_x=40.1$ MeV) in the γ_1 channel. In this case, the 90° analyzing power data for γ_1 are well described by including an $E2$ resonance with parameters $E_{\mathrm{GQR}}=38.6\pm1.0$ MeV, $\Gamma_{\mathrm{GQR}}=5.0\pm1.2$ MeV, and $S_{\mathrm{GQR}}=(50\pm15)\%$. By contrast, the γ_0 channel does not show much sensitivity to the presence of collective $E2$ strength in this energy region, and these data can be equally well described by a DSD calculation with or without an IVGQR. It is not clear whether the failure to observe an IVGQR built on the ground state is due to the insensitivity of this particular channel or to the fact that the ground state of ^{31}P does not support a compact $E2$ resonance.

The location of the $E2$ resonance built on the first excited state of ^{31}P is entirely consistent with the expected location[16,17] of the IVGQR for $A=31$: $E_{\mathrm{GQR}}\sim(120-130)A^{-1/3}\sim38-41$ MeV. Thus, the present results indicate that the collective $E2$ strength identified in the (p,γ_1) channel, as seen in the model-independent TME analysis and in the energy dependence of the 90° analyzing power, arises from the isovector giant quadrupole resonance built on the first excited state of ^{31}P.

ACKNOWLEDGMENTS

We express our deep appreciation for the patient and untiring assistance of R.-M. Larimer in all phases of the experimental measurements. We also gratefully acknowledge the generous contributions of E. B. Norman, D. J. Clark, R. J. McDonald, S. E. Kuhn, and W. Rathbun. Many thanks are due to the research staff and technical personnel of the 88-Inch Cyclotron at the Lawrence Berkeley Laboratory for their hospitality during our visits. This work was supported in part by the U.S. Department of Energy, under Contract No. DE-AC05-76ER01067.

APPENDIX

The relations between the angular distribution coefficients a_k and b_k and the transition matrix elements for capture to the first excited state of ^{31}P ($E_x=1.27$ MeV) are given below in the jj coupling scheme. The notation $^{2I+1}l_j$ is defined in the text. The analogous relations for capture to the ground state are given in Ref. 1. A detailed description of the formalism used to generate these angular momentum coupling relations is presented in Ref. 12.

The "product" of two matrix elements T and T' (where $T\equiv Re^{i\phi}$) given below is a shorthand notation representing a complex algebraic operation. For the a_k equations, the "product" TT' represents the expression $\mathrm{Re}(TT'^*)=RR'\cos(\phi'-\phi)$. For the b_k equations, the "product" TT' represents the expression $\mathrm{Re}(iTT'^*)=RR'\sin(\phi'-\phi)$.

$$1=(^2p_{1/2})^2+2(^4p_{3/2})^2+3(^6f_{5/2})^2+(^2s_{1/2})^2+2(^4d_{3/2})^2+3(^6d_{5/2})^2+4(^8g_{7/2})^2\ ,$$

$$\begin{aligned}a_1=&1.732(^2p_{1/2})(^2s_{1/2})+2.449(^2p_{1/2})(^4d_{3/2})-1.095(^4p_{3/2})(^2s_{1/2})+1.239(^4p_{3/2})(^4d_{3/2})\\&+5.217(^4p_{3/2})(^6d_{5/2})-1.138(^6f_{5/2})(^4d_{3/2})+0.913(^6f_{5/2})(^6d_{5/2})+8.606(^6f_{5/2})(^8g_{7/2})\ ,\end{aligned}$$

$$\begin{aligned}a_2=&0.632(^2p_{1/2})(^4p_{3/2})+2.324(^2p_{1/2})(^6f_{5/2})+0.800(^4p_{3/2})^2-1.470(^4p_{3/2})(^6f_{5/2})\\&-1.200(^6f_{5/2})^2+1.414(^2s_{1/2})(^4d_{3/2})-1.134(^2s_{1/2})(^6d_{5/2})+1.145(^4d_{3/2})(^6d_{5/2})\\&-1.296(^4d_{3/2})(^8g_{7/2})+0.612(^6d_{5/2})^2+1.039(^6d_{5/2})(^8g_{7/2})+2.041(^8g_{7/2})^2\ ,\end{aligned}$$

$$\begin{aligned}a_3=&1.309(^2p_{1/2})(^6d_{5/2})+3.703(^2p_{1/2})(^8g_{7/2})+1.859(^4p_{3/2})(^4d_{3/2})+2.650(^4p_{3/2})(^6d_{5/2})\\&-2.342(^4p_{3/2})(^8g_{7/2})+2.683(^6f_{5/2})(^2s_{1/2})+3.036(^6f_{5/2})(^4d_{3/2})-2.434(^6f_{5/2})(^6d_{5/2})\\&-2.869(^6f_{5/2})(^8g_{7/2})\ ,\end{aligned}$$

$$\begin{aligned}a_4=&4.276(^2s_{1/2})(^8g_{7/2})+3.665(^4d_{3/2})(^6d_{5/2})+4.320(^4d_{3/2})(^8g_{7/2})+1.959(^6d_{5/2})^2\\&-3.463(^6d_{5/2})(^8g_{7/2})-1.469(^8g_{7/2})^2\ ,\end{aligned}$$

$$b_1 = -1.732(^2p_{1/2})(^2s_{1/2}) + 1.225(^2p_{1/2})(^4d_{3/2}) - 0.548(^4p_{3/2})(^2s_{1/2}) + 2.479(^4p_{3/2})(^4d_{3/2}) - 2.608(^4p_{3/2})(^6d_{5/2}) + 0.569(^6f_{5/2})(^4d_{3/2}) - 2.738(^6f_{5/2})(^6d_{5/2}) + 4.303(^6f_{5/2})(^8g_{7/2}) ,$$

$$b_2 = -0.316(^2p_{1/2})(^4p_{3/2}) + 0.775(^2p_{1/2})(^6f_{5/2}) - 1.225(^4p_{3/2})(^6f_{5/2}) + 0.707(^2s_{1/2})(^4d_{3/2}) + 0.378(^2s_{1/2})(^6d_{5/2}) - 0.955(^4d_{3/2})(^6d_{5/2}) - 0.432(^4d_{3/2})(^8g_{7/2}) + 1.212(^6d_{5/2})(^8g_{7/2}) ,$$

$$b_3 = -0.436(^2p_{1/2})(^6d_{5/2}) + 0.926(^2p_{1/2})(^8g_{7/2}) + 0.620(^4p_{3/2})(^4d_{3/2}) - 0.221(^4p_{3/2})(^6d_{5/2}) - 1.171(^4p_{3/2})(^8g_{7/2}) - 0.894(^6f_{5/2})(^2s_{1/2}) - 0.253(^6f_{5/2})(^4d_{3/2}) + 1.217(^6f_{5/2})(^6d_{5/2}) - 0.239(^6f_{5/2})(^8g_{7/2}) ,$$

$$b_4 = 1.069(^2s_{1/2})(^8g_{7/2}) - 0.916(^4d_{3/2})(^6d_{5/2}) + 0.432(^4d_{3/2})(^8g_{7/2}) - 1.212(^6d_{5/2})(^8g_{7/2}) .$$

---

*Present address: Dept. of Physics, Duke University, Durham, NC 27706.

†Present address: Dept. of Physics, George Washington University, Washington, D.C. 20052.

[1]C. P. Cameron, R. D. Ledford, M. Potokar, D. G. Rickel, N. R. Roberson, and H. R. Weller, Phys. Rev. C **22**, 397 (1980).

[2]C. P. Cameron, Ph.D. thesis, Duke University, 1977 (unpublished).

[3]F. Saporetti and R. Guidotti, Nucl. Phys. **A390**, 207 (1982).

[4]M. A. Kovash, B. Andersen-Pugh, M. T. McEllistrem, J. K. Ternes, J. H. Trice, J. L. Weil, S. L. Blatt, H. J. Hausman, D. G. Marchlenski, and A. D. Bacher, Phys. Rev. C **40**, R1093 (1989).

[5]M. Anghinolfi, P. Corvisiero, G. Ricco, M. Sanzone, M. Taiuti, and A. Zucchiatti, Phys. Rev. C **28**, 1005 (1983).

[6]K. A. Snover, J. E. Bussoletti, K. Ebisawa, T. A. Trainor, and A. B. McDonald, Phys. Rev. Lett. **37**, 273 (1976).

[7]S. S. Hanna, H. F. Glavish, R. Avida, J. R. Calarco, E. Kuhlmann, and R. LaCanna, Phys. Rev. Lett. **32**, 114 (1974).

[8]H. R. Weller and N. R. Roberson, IEEE Trans. Nucl. Sci. **NS-28**, 1268 (1981).

[9]A. D. Bacher, G. R. Plattner, H. E. Conzett, D. J. Clark, H. Grunder, and W. F. Tivol, Phys. Rev. C **5**, 1147 (1972).

[10]P. M. Endt and C. van der Leun, Nucl. Phys. **A310**, 1 (1978).

[11]M. E. Rose, Phys. Rev. **91**, 610 (1953).

[12]R. G. Seyler and H. R. Weller, Phys. Rev. C **20**, 453 (1979).

[13]F. James and M. Roos, Comput. Phys. Commun. **10**, 343 (1975); and unpublished.

[14]F. B. Becchetti, Jr. and G. W. Greenlees, Phys. Rev. **182**, 1190 (1969).

[15]F. E. Bertrand, Annu. Rev. Nucl. Sci. **26**, 457 (1976).

[16]A. Bohr and B. R. Mottelson, *Nuclear Structure* (Benjamin, New York, 1975), Vol. II.

[17]F. E. Bertrand, Nucl. Phys. **A354**, 129c (1981).